
Article:
Mills, BJW orcid.org/0000-0002-9141-0931, Belcher, CM, Lenton, TM et al. (1 more author) (2016) A modeling case for high atmospheric oxygen concentrations during the Mesozoic and Cenozoic. Geology, 44 (12). pp. 1023-1026. ISSN 0091-7613

https://doi.org/10.1130/G38231.1

A modeling case for high atmospheric oxygen concentrations during the Mesozoic and Cenozoic

Benjamin J.W. Mills[1*], Claire M. Belcher[2], Timothy M. Lenton[2], and Robert J. Newton[1]

[1]School of Earth and Environment, University of Leeds, Leeds LS2 9JT, UK

[2]College of Life and Environmental Sciences, University of Exeter, Exeter EX4 4QE, UK

*E-mail: b.mills@leeds.ac.uk

ABSTRACT

Changes in atmospheric oxygen concentration over Earth history are commonly related to the evolution of animals and plants. But there is no direct geochemical proxy for O_2 levels, meaning that estimations rely heavily on modeling approaches. The results of such studies differ greatly, to the extent that today's atmospheric mixing ratio of 21% might be either the highest or lowest level during the past 200 m.y. Long term oxygen sources, such as the burial in sediments of reduced carbon and sulfur species, are calculated in models by representation of nutrient cycling and estimation of productivity, or by isotope mass balance (IMB)—a technique in which burial rates are inferred in order to match known isotope records. Studies utilizing these different techniques produce conflicting estimates for paleoatmospheric O_2, with nutrient-weathering models estimating concentrations close to, or above, that of the present day, and IMB models estimating low O_2, especially during the Mesozoic. Here we reassess the IMB technique using the COPSE biogeochemical model. IMB modelling is confirmed to be highly sensitive to assumed carbonate $\delta^{13}C$, and when this input is defined following recent

compilations, predicted O_2 is significantly higher and in reasonable agreement with that of non-IMB techniques. We conclude that there is no model-based support for low atmospheric oxygen concentrations during the past 200 m.y. High Mesozoic O_2 is consistent with wildfire records and the development of plant fire adaptions, but links between O_2 and mammal evolution appear more tenuous.

INTRODUCTION

Oxygen fuels the chemical reactions that take place in the mitochondria of eukaryotic cells, and pO_2 therefore places limits on the performance and survival of animals. Thus, changes in atmospheric O_2 concentration over Earth history are commonly seen as triggers for animal, and later for mammal, evolution (Lyons et al., 2014; Falkowski et al., 2005). Ratios of O_2:CO_2 determine the efficiency of photosynthesis, and variations in pO_2 dramatically influence wildfire dynamics, leading to strong potential links between pO_2 and plant evolution (He et al., 2012). But long-term variations in oxygen are difficult to estimate: the continuous presence of fossilized charcoal in sediments younger than 420 Ma indicates sufficient oxygen to sustain combustion (O_2 > 15% of the atmosphere, Belcher and McElwain, 2008), and the severity of fires in hyperoxic environments suggests that O_2 has remained below ~30% during this period (Jones and Chaloner, 1991; Belcher et al., 2010).

Between these limits, calculating variations in atmospheric oxygen relies on "forward" biogeochemical models of long-term O_2 source-and-sink processes or the interpretation of geochemical proxies (Fig. 1). Forward models can be divided into two groups, depending on how they estimate the burial rate of reduced carbon and sulfur, which are the principal sources of O_2 over geological time scales. These organically

mediated fluxes can be either estimated from the input of material and nutrients via weathering (Arvidson et al., 2013; Bergman et al., 2004; Hansen and Wallman, 2003; shown in green in Fig. 1) or inferred by comparing geological carbon and sulfur isotope records to the isotopic composition of modeled sediments (isotope mass balance [IMB]; Berner, 2009; Falkowski et al., 2005; red in Fig. 1).

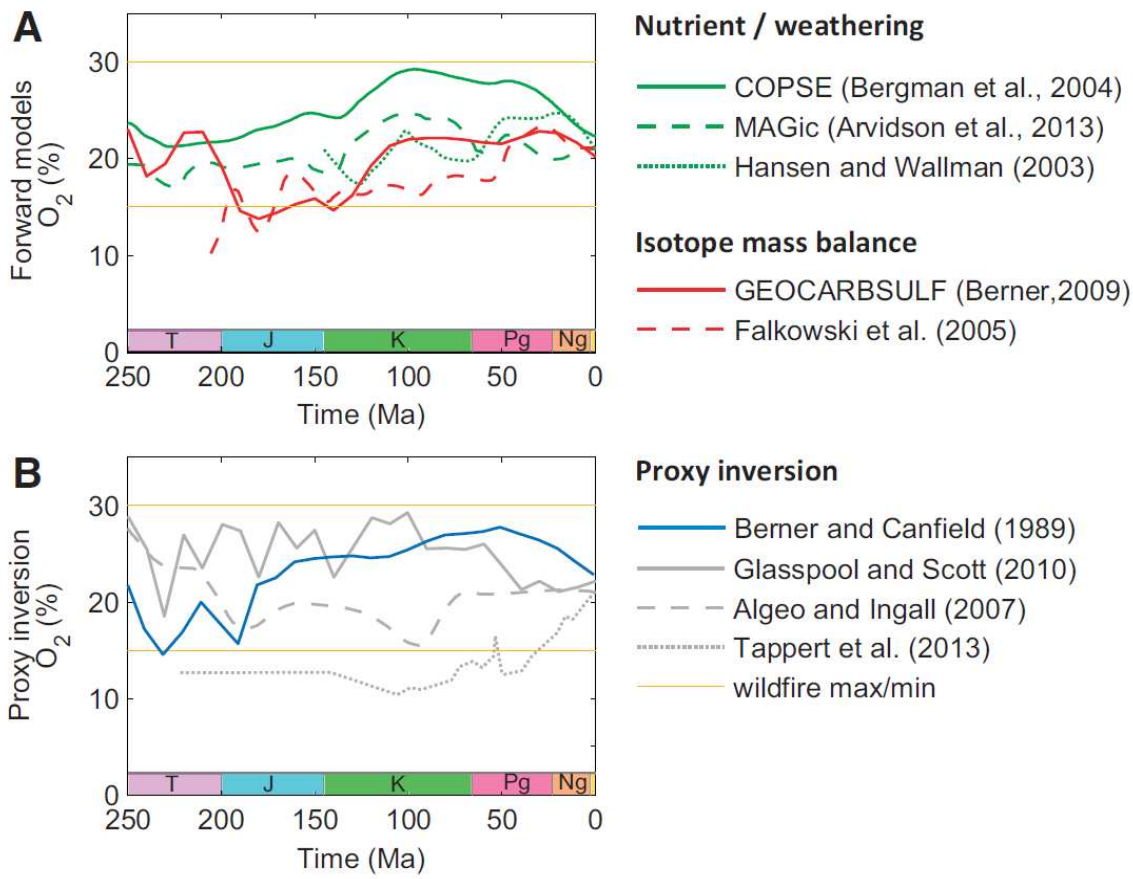

Figure 1. Reconstructions for Mesozoic and Cenozoic atmospheric O_2 mixing ratio. A: Forward models of O_2 sources and sinks (green lines) and isotope mass balance models (red lines). B: Proxy inversion assuming relationships between O_2 concentration and either fossil charcoal abundance (Glasspool and Scott, 2010), carbon-to-phosphorus ratios in sediments (Algeo and Ingall, 2007), carbon isotope composition of plant resins (Tappert et al., 2013), or combined estimates for sedimentation rate and abundance of

organic carbon and pyrite in rock samples (Berner and Canfield, 1989). Also shown: wildfire minimum and maximum (see text). T—Triassic; J—Jurassic; K—Cretaceous; Pg—Paleogene; Ng—Neogene.

Estimates of O_2 differ greatly between different forward models. Nutrient and weathering models typically predict higher values, while IMB models predict low pO_2 during the Mesozoic, potentially in conflict with the evidence for widespread fires (Belcher and McElwain, 2008). All models show general agreement for a gradual rise in pO_2 during the Cretaceous, although they disagree on whether this was a rise from low O_2 toward present values, or a rise from present to superambient levels, followed by a decline over the Cenozoic.

"Proxy inversion" methods estimate atmospheric oxygen by reference to geochemical data. Glasspool and Scott (2010) assumed a correlation between the abundance of charcoal in mires and atmospheric oxygen, scaling to the present-day value, and assumed a Permian-Carboniferous O_2 maximum of 30%. Algeo and Ingall (2007) related C_{org}:P (org—organic) ratios in organic-rich sediments to benthic redox conditions, and therefore to global atmospheric O_2 levels, scaling to the fire window. The "rock abundance" method of Berner and Canfield (1989) utilizes the carbon and sulfur contents of ancient sediments as well as sedimentation rate to infer oxygen production rates, linking this to pO_2. Tappert et al. (2013) inferred pO_2 from measured plant resin $\delta^{13}C$ and CO_2 proxies, reasoning that plant $\delta^{13}C$ reflects the CO_2:O_2 ratio of the growth environment. This technique produces very low estimates and is subject to high uncertainty in quantifying the plant $\delta^{13}C$ response to global O_2 and CO_2 variations.

The level of disagreement in current O_2 reconstructions is extreme and is masked to some degree by the scaling of many results to the fire window. This makes it difficult to assess the role of oxygen in the evolution of plants and animals during the Mesozoic and Cenozoic. Moreover, the forward models discussed here are commonly applied in studies of Paleozoic and Precambrian oxygen shifts (Clapham and Karr, 2012; Lenton and Watson, 2004), with important implications for the evolution of animals and land plants.

In this paper, we focus on the question of whether atmospheric oxygen concentration over the past 200 m.y. has been generally below or above the present-day value. We address this by exploring the isotope mass balance technique, which currently produces the most reliable and widely cited evidence for low Mesozoic oxygen.

FORWARD MODELING OF PALEOATMOSPHERIC OXYGEN CONCENTRATION

Forward models are based on the long-term carbon and sulfur cycles (e.g., Kump and Garrels, 1986), as shown in Figure 2. These systems consider atmospheric and oceanic carbon (A) and sulfur (S) and the much larger sedimentary reservoirs of oxidized and reduced species. The crustal reservoirs can be split into young (y) and ancient (a) sediments, with the assumption that the young reservoirs are smaller and constitute the majority of interaction with the surface system. This “rapid recycling” permits the isotopic signature of the young reservoirs to change more quickly and has a buffering effect when burial rates are calculated via isotope mass balance (Berner, 1987, 2009).

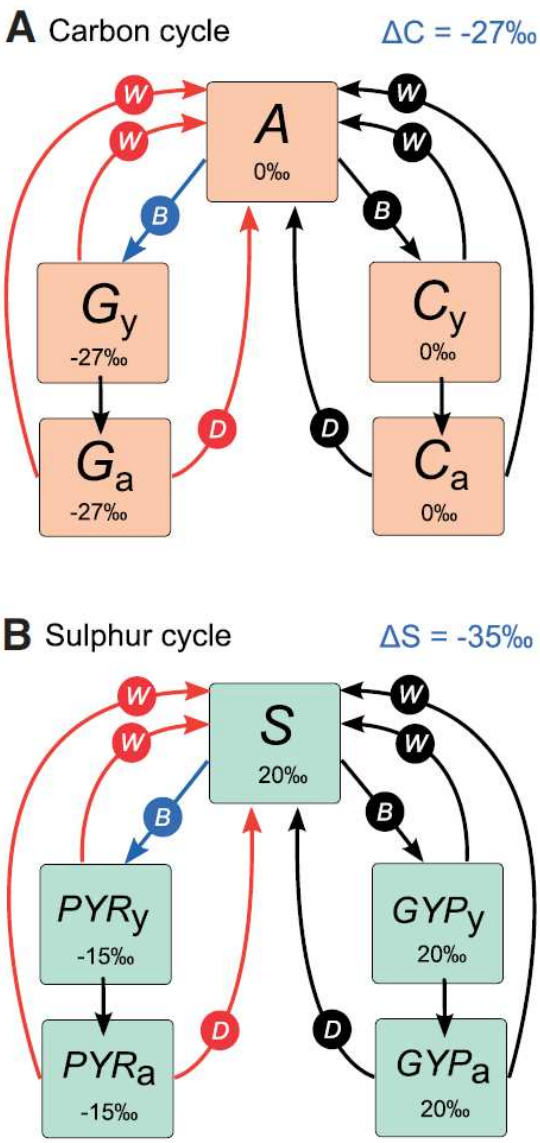

Figure 2. Long-term carbon and sulfur cycles. Carbon cycle consists of fluxes between atmospheric and oceanic carbon (A), organic carbon (G), and carbonate (C). Sulfur cycle represents oceanic sulfate (S), buried pyrite (PYR), and gypsum (GYP). Burial (B) moves carbon and sulfur from the atmosphere and ocean to the crustal reservoirs, and it is returned by weathering (W) and degassing and metamorphism (D). *Subscript "y"* denotes young crustal *reservoirs, "a"* denotes ancient crustal reservoirs. Oxygen sources are shown in blue, sinks are shown in red. Other processes shown in black. Present-day isotope ratios δ^{13}C and δ^{34}S are shown for *carbon and sulfur reservoirs respectively in per mil (‰)*; ΔC and ΔS show the burial fractionation effects for carbon and sulfur, respectively.

Oxygen sources are the burial (B) of photosynthetically derived carbon and of pyrite sulfur (blue arrows in Fig. 2). Burial of these reduced species results in oxygenation of the surface environment. The buried species are eventually uplifted and

weathered (W) or are returned to the surface via metamorphism and degassing (D), which represent oxygen sinks (red in Fig. 2). The source-sink balance for O_2 is:

$$\frac{dO_2}{dt} = B(G) - W(G_y) - W(G_a) - D(G_a) + 2\left[B(PYR) - W(PYR_y) - W(PYR_a) - D(PYR_a)\right], \quad (1)$$

where G is organic carbon and PYR is buried pyrite.

Models calculate these fluxes, informed by internal parameters such as temperature, rates of erosion and degassing, rock exposure, and biological processes (Berner, 2006; Bergman et al., 2004). Burial, weathering, and degassing of the oxidized forms of carbon and sulfur (black arrows in Fig. 2) do not impact oxygen concentration directly but do affect the size and isotopic composition of the surface reservoirs (A, S), so cannot be ignored.

Isotope Mass Balance

Organic carbon and pyrite sulfur are isotopically lighter than the CO_2 and SO_4 they are derived from, due to kinetic selection during photosynthesis and sulfate reduction. The canonical isotope ratios for the present-day system (Hayes et al., 1999) are shown in Figure 2, alongside the fractionation effects ΔC (carbon) and ΔS (sulfur). These isotopic compositions and fractionation effects have changed over Earth history. For example, increasing the burial rate of organic, isotopically depleted carbon would act to increase the isotope ratio $\delta^{13}C$ in the parent surface reservoir A.

Assuming that buried carbonates and sulfates reflect ancient oceanic isotopic composition, the geological $\delta^{13}C$ and $\delta^{34}S$ records can be used to back-calculate the required rate of burial of organic carbon and pyrite sulfur and therefore the rate of oxygen production (Berner, 1987). This requires knowledge of the input fluxes via weathering

and degassing (W, D), the isotopic composition of the crustal reservoirs, and the fractionation effects ΔC and ΔS. The isotope mass balance equations consider isotopic inputs and outputs and are rearranged to calculate burial rates. The mass balance for the carbon system is shown below, and the sulfur system follows the same structure. See Berner (1987) and Berner (2001) for detailed descriptions. Here δ(X) is the isotopic composition of reservoir X:

$$B(G) = \frac{1}{\Delta C}\{[\delta(A) - \delta(G_{\mathrm{y}})]W(G_{\mathrm{y}}) + [\delta(A) - \delta(G_{\mathrm{a}})][W(G_{\mathrm{a}}) + D(G_{\mathrm{a}})] + [\delta(A) - \delta(C_{\mathrm{y}})]W(C_{\mathrm{y}}) + [\delta(A) - \delta(C_{\mathrm{a}})][W(C_{\mathrm{a}}) + D(C_{\mathrm{a}})]\}\ . \quad (2)$$

The GEOCARBSULF model (Berner, 2006, 2009; Fig. 1A) combines the isotope mass balance technique with calculations for biogeochemical carbon and sulfur fluxes, and is generally considered the current "best-guess" atmospheric O_2 prediction. Error analysis of the GEOCARBSULF model (Royer et al., 2014) plots model predictions for variation in all input parameters and robustly predicts low Mesozoic O_2. However, this study is hampered by high model failure rate (the model crashes when some inputs are changed significantly from their default values), allowing only minimal variation of the $\delta^{13}C$ input [δ(A) in Equation 2], far from the uncertainty in global records.

The IMB-COPSE Model

We re-evaluate the oxygen predictions via isotope mass using the revised COPSE model (Mills et al., 2014). COPSE is a derivative of the GEOCARB models and uses many of the same calculations, but it differs from GEOCARBSULF in several ways that make it potentially more useful for evaluating O_2 predictions: the model is solved numerically using an implicit variable order method (Shampine and Reichelt, 1997), which greatly reduces model failure rate and allows testing of different $\delta^{13}C$ inputs. The

model also integrates recent research on the global rate of CO_2 degassing and the weathering of volcanic rocks (Van Der Meer et al., 2014; Mills et al., 2014), which has not previously been applied to oxygen calculation.

The standard COPSE model includes nutrient cycles in order to estimate productivity and calculate the fluxes of organic carbon and pyrite sulfur burial. In this exploration (IMB-COPSE), the nutrient cycles are removed and the productivity and burial calculations are replaced with the standard isotope mass balance equations (Berner, 2001; Equation 2), following their incorporation into GEOCARBSULF (Berner, 2006). This includes the addition of rapid recycling. See the GSA Data Repository[1] for full model description.

MODEL INPUTS AND RESULTS

Initially the IMB-COPSE model is run using the GEOCARBSULF $\delta^{13}C$ and $\delta^{34}S$ inputs (red dashed line in Fig. 3A). Despite the differences in model weathering and degassing processes, the IMB-COPSE model produces O_2 predictions that are strikingly similar to those of GEOCARBSULF (black and red lines in Fig. 3B). This includes a prolonged period of low atmospheric O_2 during the Jurassic and Early Cretaceous.

We explore model sensitivity to assumed $\delta^{13}C$ and $\delta^{34}S$ records by removing the GEOCARBSULF inputs and replacing them with values from recent literature compilations. Current records for Phanerozoic $\delta^{34}S$ (Algeo et al., 2015) do not differ greatly from the GEOCARBSULF inputs, and their substitution has little impact on model predictions (see the Data Repository). Recent compilations of carbonate $\delta^{13}C$, however, show notable differences from the curves used in GEOCARBSULF.

The $\delta^{13}C$ compilation of Saltzman and Thomas (2012; denoted GTS2012) is shown in blue in Figure 3A. The solid line shows the moving average, and dashed lines show ±1σ over 5 m.y. bins. The Mesozoic record is at higher resolution than the GEOCARBSULF input but does not show substantial base-level differences. The GTS2012 curve incorporates recent Cenozoic data from benthic foraminifera (Cramer et al., 2009), which agrees with the bulk record of $\delta^{13}C$ in pelagic carbonates (Katz et al., 2005) in giving a present-day oceanic $\delta^{13}C$ value close to 0‰, whereas the GEOCARBSULF curve has a present-day value closer to 2‰. This value is extremely important in isotope mass balance modeling as it sets the relative state of the system as we explore ancient time periods. During the Jurassic period, the GEOCARBSULF curve assumes a global ocean $\delta^{13}C$ signature that is isotopically lighter than at present, potentially indicative of lower organic carbon burial and less oxygen production. The GTS2012 curve, however, shows a generally heavier signal than at present.

These differences in assumed oceanic $\delta^{13}C$ translate into large differences in model O_2 predictions, which tend to follow this input qualitatively. Under the GTS2012 input, the average predicted O_2 concentration (blue in Fig. 3B) remains at or above present values during the past 200 m.y., resolving the conflict with nutrient- and weathering-based models and with the wildfire minimum. Note that the O_2 predictions for the ±1σ $\delta^{13}C$ inputs cross each other due to the present-day O_2 constraint. See the Data Repository for further model uncertainty estimates, including constraints on the sulfur cycle.

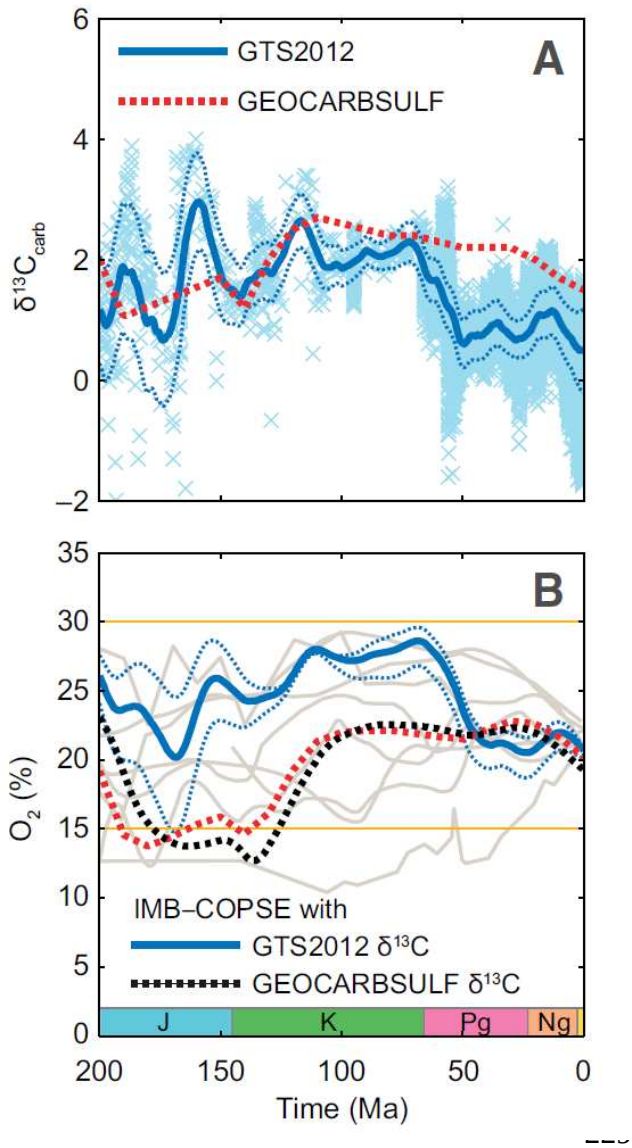

Figure 3. Results of isotope mass balance (IMB)-COPSE model. A: δ^{13}C input follows Geological Time Scale 2012 (GTS2012) (Saltzman and Thomas, 2012; blue; crosses show data points, solid line shows moving average, and dashed lines show ±1σ) or GEOCARBSULF model (Berner, 2009; red). B: Oxygen mixing ratios (%) predicted by IMB-COPSE model given δ^{13}C input from GTS2012 (blue) or GEOCARBSULF (black dashed), compared to GEOCARBSULF O_2 output (red). Estimates from Figure 1 shown in gray, with fire window in orange. For full model output see Data Repository (see footnote 1). J—Jurassic; K—Cretaceous; Pg—Paleogene; Ng—Neogene.

DISCUSSION

Examination of IMB modeling confirms that the predicted rate of burial of organic carbon (the largest source of O_2) is heavily dependent on the assumed carbon

isotope record and much less dependent on other model processes, meaning that assumptions about the variation in oceanic $\delta^{13}C$ are critical in determining pO_2.

Compiling the global record of average whole-ocean $\delta^{13}C$ is difficult, as differences exist across species, depth, and temperature (Saltzman and Thomas, 2012; Cramer et al., 2009). The paleogeographic source of information at different times adds further uncertainty: in sediments older than the Early Cretaceous the majority of records are sourced from epeiric seas rather than open-ocean margins or the deep ocean. A variety of studies have shown that ancient epeiric-sea water masses could develop isotopic signatures distinct from those of the open ocean for a number of isotope systems including carbon (Coulson et al., 2011; Panchuk et al., 2006; Newton et al., 2011).

These sources of uncertainty and variability lead to significant uncertainty in the overall curve, and crucially, in whether the present-day value is lower or higher than average values over the Mesozoic and Cenozoic. Current GEOCARBSULF model predictions of low Mesozoic pO_2 rely on the assumption that modern oceanic $\delta^{13}C$ values are higher than those during the Mesozoic, which is not shown in recent records based on either bulk-rock (Katz et al., 2005) or single-organism (Cramer et al., 2009) compilations. We therefore conclude that there is no model-based support for low Mesozoic pO_2 concentrations.

Taking our results together with the forward modeling approaches that calculate oxygen production via weathering and nutrient systems (Fig. 1), we argue for high O_2 during the Mesozoic and Cenozoic, with a rise to above-modern oxygen concentrations during the Cretaceous. This view is compatible with the limits of combustion (Belcher and McElwain, 2008). Low-oxygen predictions are not a necessary consequence of

isotope mass balance modeling, while estimations based on the $\delta^{13}C$ composition of plant material (Tappert et al., 2013) are extremely difficult to validate due to the high variability of measured values and absence of controlled growth experiments in different CO_2:O_2 ratios.

Linking variations in oxygen concentration to animal evolution is speculative, and it is difficult to separate ecological and climatic drivers (Smith et al., 2010; Clapham and Karr, 2012). Proxies for O_2 based on plant flammability are useful, but must be expanded to consider linkages between pO_2 and fire-adapted trait selection (e.g., He et al., 2012, 2015; Lamont and Downes, 2011). Reconstructing atmospheric oxygen via modeling studies depends greatly on the ability to accurately compile average, whole-ocean $\delta^{13}C$ for the ancient past, whether this record is used to directly drive the model (IMB) or as a means of comparison to model outputs. It is clear that modelers and paleontologists should seek to work together if we are to better explore the links between oxygen and evolution.

ACKNOWLEDGMENTS

We thank the late R.A. Berner for the GEOCARBSULF model code, and M.R. Saltzman and E. Thomas for isotope data. Mills is funded by a University of Leeds Academic Fellowship; Belcher acknowledges funding from European Research Council Starter Grant ERC-2013-StG-335891-ECOFLAM. Lenton acknowledges funding from the Leverhulme Trust (RPG-2013-106). We thank Noah Planavsky and two anonymous reviewers for assessing this work.

REFERENCES CITED

Algeo, T.J., and Ingall, E., 2007, Sedimentary C_{org}:P ratios, paleocean ventilation, and Phanerozoic atmospheric pO_2: Palaeogeography, Palaeoclimatology, Palaeoecology, v. 256, p. 130–155, doi:10.1016/j.palaeo.2007.02.029.

Algeo, T.J., Luo, G.M., Song, H.Y., Lyons, T.W., and Canfield, D.E., 2015, Reconstruction of secular variation in seawater sulfate concentrations: Biogeosciences, v. 12, p. 2131–2151, doi:10.5194/bg-12-2131-2015.

Arvidson, R.S., Mackenzie, F.T., and Guidry, M.W., 2013, Geologic history of seawater: A MAGic approach to carbon chemistry and ocean ventilation: Chemical Geology, v. 362, p. 287–304, doi:10.1016/j.chemgeo.2013.10.012.

Belcher, C.M., and McElwain, J.C., 2008, Limits for combustion in low O_2 redefine paleoatmospheric predictions for the Mesozoic: Science, v. 321, p. 1197–1200, doi:10.1126/science.1160978.

Belcher, C.M., Yearsley, J.M., Hadden, R.M., McElwain, J.C., and Rein, G., 2010, Baseline intrinsic flammability of Earth's ecosystems estimated from paleoatmospheric oxygen over the past 350 million years: Proceedings of the National Academy of Sciences of the United States of America, v. 107, p. 22,448–22,453, doi:10.1073/pnas.1011974107.

Bergman, N.M., Lenton, T.M., and Watson, A.J., 2004, COPSE: A new model of biogeochemical cycling over Phanerozoic time: American Journal of Science, v. 304, p. 397–437, doi:10.2475/ajs.304.5.397.

Berner, R.A., 1987, Models for carbon and sulfur cycles and atmospheric oxygen: Application to Paleozoic geologic history: American Journal of Science, v. 287, p. 177–196, doi:10.2475/ajs.287.3.177.

Berner, R.A., 2001, Modelling atmospheric O_2 over Phanerozoic time: Geochimica et Cosmochimica Acta, v. 65, p. 685–694, doi:10.1016/S0016-7037(00)00572-X.

Berner, R.A., 2006, GEOCARBSULF: A combined model for Phanerozoic atmospheric O_2 and CO_2: Geochimica et Cosmochimica Acta, v. 70, p. 5653–5664, doi:10.1016/j.gca.2005.11.032.

Berner, R.A., 2009, Phanerozoic atmospheric oxygen: New results using the GEOCARBSULF model: American Journal of Science, v. 309, p. 603–606, doi:10.2475/07.2009.03.

Berner, R.A., and Canfield, D.E., 1989, A new model for atmospheric oxygen over Phanerozoic time: American Journal of Science, v. 289, p. 333–361, doi:10.2475/ajs.289.4.333.

Clapham, M.E., and Karr, J.A., 2012, Environmental and biotic controls on the evolutionary history of insect body size: Proceedings of the National Academy of Sciences of the United States of America, v. 109, p. 10,927–10,930, doi:10.1073/pnas.1204026109.

Coulson, A.B., Kohn, M.J., and Barrick, R.E., 2011, Isotopic evaluation of ocean circulation in the Late Cretaceous North American seaway: Nature Geoscience, v. 4, p. 852–855, doi:10.1038/ngeo1312.

Cramer, B.S., Toggweiler, J.R., Wright, J.D., Katz, M.E., and Miller, K.G., 2009, Ocean overturning since the Late Cretaceous: Inferences from a new benthic foraminiferal isotope compilation: Paleoceanography, v. 24, PA4216, doi:10.1029/2008PA001683.

Falkowski, P.G., Katz, M.E., Milligan, A.J., Fennel, K., Cramer, B.S., Aubry, M.P., Berner, R.A., Novacek, M.J., and Zapol, W.M., 2005, The rise of oxygen over the

past 205 million years and the evolution of large placental mammals: Science, v. 309, p. 2202–2204, doi:10.1126/science.1116047.

Glasspool, I.J., and Scott, A.C., 2010, Phanerozoic concentrations of atmospheric oxygen reconstructed from sedimentary charcoal: Nature Geoscience, v. 3, p. 627–630, doi:10.1038/ngeo923.

Hansen, K.W., and Wallman, K., 2003, Cretaceous and Cenozoic evolution of seawater composition, atmospheric O_2 and CO_2: A model perspective: American Journal of Science, v. 303, p. 94–148, doi:10.2475/ajs.303.2.94.

Hayes, J.M., Strauss, H., and Kaufman, A.J., 1999, The abundance of ^{13}C in marine organic matter and isotopic fractionation in the global biogeochemical cycle of carbon during the past 800 Ma: Chemical Geology, v. 161, p. 103–125, doi:10.1016/S0009-2541(99)00083-2.

He, T., Pausas, J.G., Belcher, C.M., Schwilk, D.W., and Lamont, B.B., 2012, Fire-adapted traits of Pinus arose in the fiery Cretaceous: The New Phytologist, v. 194, p. 751–759, doi:10.1111/j.1469-8137.2012.04079.x.

He, T., Belcher, C.M., Lamont, B.B., and Lim, S.L., 2015, A 350-million-year legacy of fire adaption among conifers: Journal of Ecology, v. 104, p. 352–363, doi:10.1111/1365-2745.12513.

Jones, T., and Chaloner, W., 1991, Fossil charcoal, its recognition and palaeoatmospheric significance: Palaeogeography, Palaeoclimatology, Palaeoecology, v. 97, p. 39–50, doi:10.1016/0031-0182(91)90180-Y.

Katz, M.E., Wright, J.D., Miller, K.G., Cramer, B.S., Fennel, K., and Falkowski, P.G., 2005, Biological overprint of the geological carbon cycle: Marine Geology, v. 217, p. 323–338, doi:10.1016/j.margeo.2004.08.005.

Kump, L.R., and Garrels, R.M., 1986, Modeling atmospheric O_2 in the global sedimentary redox cycle: American Journal of Science, v. 286, p. 337–360, doi:10.2475/ajs.286.5.337.

Lamont, B.B., and Downes, S., 2011, Fire-stimulated flowering among resprouters and geophytes in Australia and South Africa: Plant Ecology, v. 212, p. 2111–2125, doi:10.1007/s11258-011-9987-y.

Lenton, T.M., and Watson, A.J., 2004, Biotic enhancement of weathering, atmospheric oxygen and carbon dioxide in the Neoproterozoic: Geophysical Research Letters, v. 31, L05202, doi:10.1029/2003GL018802.

Lyons, T.W., Reinhard, C.T., and Planavsky, N.J., 2014, The rise of oxygen in Earth's early ocean and atmosphere: Nature, v. 506, p. 307–315, doi:10.1038/nature13068.

Mills, B., Daines, S.J., and Lenton, T.M., 2014, Changing tectonic controls on the long-term carbon cycle from Mesozoic to present: Geochemistry Geophysics Geosystems, v. 15, p. 4866–4884, doi:10.1002/2014GC005530.

Newton, R.J., Reeves, E.P., Kafousia, N., Wignall, P.B., Bottrell, S.H., and Sha, J.G., 2011, Low marine sulfate concentrations and the isolation of the European epicontinental sea during the Early Jurassic: Geology, v. 39, p. 7–10, doi:10.1130/G31326.1.

Panchuk, K.M., Holmden, C.E., and Leslie, S.A., 2006, Local controls on carbon cycling in the Ordovician midcontinent region of North America, with implications for

carbon isotope secular curves: Journal of Sedimentary Research, v. 76, p. 200–211, doi:10.2110/jsr.2006.017.

Royer, D.L., Donnadieu, Y., Park, J., Kowalczyk, J., and Godderis, Y., 2014, Error analysis of CO_2 and O_2 estimates from the long-term geochemical model GEOCARBSULF: American Journal of Science, v. 314, p. 1259–1283, doi:10.2475/09.2014.01.

Saltzman, M.R., and Thomas, E., 2012, Carbon isotope stratigraphy, in Gradstein, F.M., et al., eds., The Geological Time Scale 2012: Boston, Elsevier, p. 207–232, doi:10.1016/B978-0-444-59425-9.00011-1.

Shampine, L.F., and Reichelt, M.W., 1997, The MATLAB ODE suite: SIAM Journal on Scientific Computing, v. 18, p. 1–22, doi:10.1137/S1064827594276424.

Smith, F.A., et al., 2010, The evolution of maximum body size of terrestrial mammals: Science, v. 330, p. 1216–1219, doi:10.1126/science.1194830.

Tappert, R., McKellar, R.C., Wolfe, A.P., Tappert, M.C., Ortega-Blanco, J., and Muehlenbachs, K., 2013, Stable carbon isotopes of C_3 plant resins and ambers record changes in atmospheric oxygen since the Triassic: Geochimica et Cosmochimica Acta, v. 121, p. 240–262, doi:10.1016/j.gca.2013.07.011.

Van Der Meer, D.G., Zeebe, R.E., Hinsbergen, D.J.J.V., Sluijs, A., Spakman, W., and Torsvik, T.H., 2014, Plate tectonic controls on atmospheric CO_2 levels since the Triassic: Proceedings of the National Academy of Sciences of the United States of America, v. 111, p. 4380–4385, doi:10.1073/pnas.1315657111.

[1]GSA Data Repository item 2016xxx, is available online at http://www.geosociety.org/pubs/ft2016.htm or on request from editing@geosociety.org. Mills_2016_O2.xlsx: Datafile of oxygen reconstructions from the IMB-COPSE model.

APPENDIX

APPENDIX 1: ALTERATIONS TO PREVIOUSLY PUBLISHED MODEL

The COPSE and GEOCARB models

The original COPSE model (Bergman et al., 2004) is a long term biogeochemical box model, based on the GEOCARB models (Berner 1991, 1994, Berner and Kothavala, 2001). It calculates fluxes between the atmosphere/ocean and sedimentary reservoirs of oxidised and reduced carbon and sulphur to estimate changes in CO_2, O_2 and ocean sulphate over the Phanerozoic. Since publication of COPSE, GEOCARB has been extended to include calculations for the sulphur cycle and oxygen (GEOCARBSULF). In Mills et al. (2014), COPSE was updated to consider the weatherable area of different rock types, and to investigate alternative reconstructions for volcanic degassing rates (Van Der Meer et al., 2014). The model predictions were compared to variation in seawater $^{87}Sr/^{86}Sr$.

The critical difference between COPSE and GEOCARBSULF is the method used to estimate the burial rates of organic carbon and pyrite sulphur, which are the long term sources of oxygen. COPSE uses integrated cycles of limiting nutrients P and N (following Lenton and Watson 2000) to estimate these fluxes based on other model parameters, such as nutrient delivery via weathering. GEOCARBSULF uses an isotope mass balance technique (IMB: Berner 1987, 2001) which infers the burial rates from

known changes in isotope ratios $\delta^{13}C$ and $\delta^{34}S$, and does not require the calculation of nutrient fluxes. Whist model predictions for CO_2 over the Phanerozoic are broadly similar, predictions for variation in O_2 are substantially different.

Model used in this work

This paper uses the latest version of the COPSE biogeochemical model (Mills et al., 2014), and adds to this a routine for calculating the burial rates of organic carbon and pyrite sulphur via isotope mass balance, mirroring the functionality of the GEOCARBSULF model (Berner, 2006; 2009). The resulting model is very similar to GEOCARBSULF, but differences remain in the assumed rate of volcanic degassing, and the weatherable area of volcanic rocks, as well as more minor quantitative differences in the calculations for weathering fluxes.

In this paper we wish to test the oxygen predictions from the isotope mass balance system, particularly with regard to the input of $\delta^{13}C$ data, which shows large uncertainty. In theory, this test can be carried out using the GEOCARBSULF model, however recent work has shown that the computational algorithm used to solve the model fails when $\delta^{13}C$ inputs are varied only slightly from the model baseline (Royer et al., 2014). The COPSE algorithm uses a variable time-step method and is therefore suited to testing wide differences in input parameters. Thus we adapt the COPSE model to test the isotope mass balance method by removing the nutrient system and replacing with the IMB equations. This has the additional benefit of testing whether the differences in the COPSE formulations for degassing and weathering have much impact on the model outputs under isotope mass balance.

To summarize the results of this exercise:

- Replacing the nutrient system in COPSE with the exact isotope mass balance system from GEOCARBSULF (including standard inputs for $\delta^{13}C$ and $\delta^{34}S$) results in oxygen predictions very similar to GEOCARBSULF. Showing that O_2 predictions are much more dependent on the assumed isotope record than other model processes.

- Replacing the standard $\delta^{13}C$ input compilation with a more recent record (Saltzman and Thomas, 2012) results in major revision of the O_2 predictions, with $pO_2 > 0.2$atm for the whole model timeframe (200-0Ma).

Rapid recycling

In order to add the isotope mass balance system to COPSE, the model must be modified to include 'rapid recycling' of sedimentary carbon and sulphur. Under this method, it is assumed that geologically young sedimentary rocks constitute the majority of interaction with the surface system, allowing the isotopic signature of buried material to be more quickly recycled to the atmosphere and oceans. This technique has been included in all isotope mass balance approaches (Berner 1987; 2006; 2009; Royer et al., 2014).

The method involves splitting the sedimentary reservoirs for organic carbon, carbonates, pyrite and gypsum sulphur into 'young' and 'ancient' boxes. The young boxes are smaller and have higher weathering rates, the ancient boxes are much larger and have lower weathering rates (see ms figure 2). The relative size of the young and ancient reservoirs, as well as the relative weathering contributions are taken directly from

GEOCARBSULF, and are listed below with the other model parameters. The carbon and sulphur cycle schematic from the attached manuscript, which details the flux names, is reproduced here (A1) for convenience.

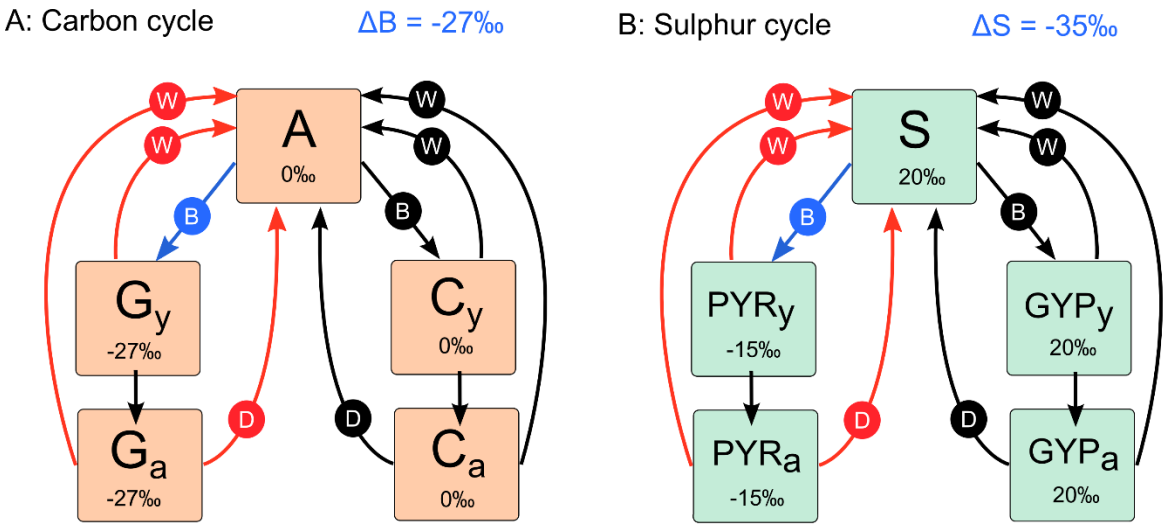

Figure A1. Long term carbon and sulphur cycles. The carbon cycle consists of fluxes between atmosphere and ocean carbon (A), organic carbon (G) and carbonate (C). The sulphur cycle represents ocean sulphate (S), buried reduced pyrite (PYR) and oxidised gypsum (GYP). Burial (B) moves carbon and sulphur from the atmosphere and ocean to the crustal reservoirs, and it is returned by weathering (W) and degassing/metamorphism (D). Subscript (y) denotes young crustal reservoirs, (a) denotes ancient crustal reservoirs. Oxygen sources are shown in blue, sinks are shown in red. Present day *isotope ratios* $\delta^{13}C$ *and* $\delta^{34}S$ are shown for carbon and sulphur reservoirs respectively in per mil *(‰), ΔB and ΔS show the burial fractionation effects for carbon and sulphur* respectively.

Isotope mass balance equations for burial fluxes

With rapid recycling added to the COPSE model, and the nutrient system removed completely, the equations representing organic carbon burial and pyrite sulphur burial are copied exactly from GEOCARBSULF, the code for which was kindly sent by R. A. Berner. The mathematical derivation is published in Berner (1987) and begins with the assumption of input-output parity for ^{12}C and ^{13}C atoms (and ^{34}S and ^{32}S for sulphur). For Carbon:

$$Input \times \delta(Input) = Output \times \delta(Output) \quad (1)$$

$$W(G_y)\delta(G_y) + W(G_a)\delta(G_a) + D(G_a)\delta(G_a) + W(C_y)\delta(C_y) + W(C_a)\delta(C_a) + D(C_a)\delta(C_a) = B(G)(\delta(A) - \Delta B) + B(C)\delta(A) \quad (2)$$

Rearranging gives:

$$\Delta B \times B(G) = \left(\delta(A) - \delta(G_y)\right) W(G_y) + \left(\delta(A) - \delta(G_a)\right)\left(W(G_a) + D(G_a)\right) + \left(\delta(A) - \delta(C_y)\right)W(C_y) + (\delta(A) - \delta(C_a))\left(W(C_a) + D(C_a)\right) \quad (3)$$

Where δ(X) is the isotopic composition of reservoir X, W denotes weathering, D denotes degassing and B denotes burial. ΔB and ΔS are the fractionation effects for burial of carbon and sulphur respectively. This equation is mirrored for the sulphur cycle.

APPENDIX 2: FULL MODEL DESCRIPTION

The full model equations are detailed below. Aside from the addition of rapid recycling and isotope mass balance, and the removal of the nutrient system, they follow

exactly the model from Mills et al., (2014). The flux names from the manuscript are simplified here for convenience:

$W(C_y) = carbw_y$, $W(C_a) = carbw_a$, $W(G_y) = oxidw_y$, $W(G_a) = oxidw_a$,

$D(C) = ccdeg$, $D(G) = ocdeg$, $B(G) = ocb$, $B(C) = mccb$

$W(GYP_y) = gypw_y$, $W(GYP_a) = gypw_a$, $W(PYR_y) = pyrw_y$, $W(PYR_a) = pyrw_a$,

$D(GYP) = gypdeg$, $D(PYR) = pyrdeg$, $B(GYP) = mgsb$, $B(PYR) = mpsb$

Reservoir calculations:

Atmosphere/ocean carbon:

$$\frac{dA}{dt} = ccdeg + carbw_y + carbw_a + oxidw_y + oxidw_a + ocdeg - mccb - ocb - sfw \quad (4)$$

Ocean sulphate:

$$\frac{dS}{dt} = pyrw_y + pyrw_a + pyrdeg + gypw_y + gypw_y + gypdeg - mpsb - mgsb \quad (5)$$

Buried organic C (young): $\frac{dG_y}{dt} = ocb - oxidw_y - F_{Gya}$ (6)

Buried organic C (ancient): $\frac{dG_a}{dt} = F_{Gya} - oxidw_a - ocdeg$ (7)

Buried carbonate C (young): $\frac{dC_y}{dt} = mccb - carbw_y - F_{Cya}$ (8)

Buried carbonate C (ancient): $\frac{dC_a}{dt} = F_{Cya} - carbw_a - ccdeg$

(9)

Buried pyrite S (young): $\frac{dPYR_y}{dt} = mpsb - pyrw_y - F_{PYRya}$

(10)

Buried pyrite S (ancient): $\frac{dPYR_a}{dt} = F_{PYRya} - pyrw_a - pyrdeg$

(11)

Buried gypsum S (young): $\frac{dGYP_y}{dt} = mgsb - gypw_y - F_{GYPya}$

(12)

Buried gypsum S (ancient): $\frac{dGYP_a}{dt} = F_{GYPya} - gypw_a - gypdeg$

(13)

Isotope reservoir calculations:

Atmosphere/ocean carbon:

$$\frac{d(A \times \delta(A))}{dt} = ccdeg \times \delta(C_a) + carbw_y \times \delta(C_y) + carbw_a \times \delta(C_a) + oxidw_y \times \delta(G_y) + oxidw_a \times \delta(G_a) + ocdeg \times \delta(G_a) - ocb \times (\delta(A) - \Delta B) - mccb \times \delta(A) - sfw \times \delta(A)$$

(14)

Ocean sulphate:

$$\frac{d(S \times \delta(S))}{dt} = gypdeg \times \delta(GYP_a) + gypw_y \times \delta(GYP_y) + gypw_a \times \delta(GYP_a) + pyrw_y \times \delta(PYR_y) + pyrw_a \times \delta(PYR_a) + pyrdeg \times \delta(PYR_a) - mpsb \times (\delta(S) - \Delta S) - mgsb \times \delta(S)$$

(15)

Buried organic C (young):

$$\frac{d(G_y \times \delta(G_y))}{dt} = ocb \times (\delta(A) - \Delta B) - oxidw_y \times \delta(G_y) - F_{Gya} \times \delta(G_y)$$

(16)

Buried organic C (ancient):

$$\frac{d(G_a \times \delta(G_a))}{dt} = F_{Gya} \times \delta(G_y) - oxidw_a \times \delta(G_a) - ocdeg \times \delta(G_a)$$

(17)

Buried carbonate C (young):

$$\frac{d(C_y \times \delta(C_y))}{dt} = mccb \times \delta(A) - carbw_y \times \delta(C_y) - F_{Cya} \times \delta(C_y)$$

(18)

Buried carbonate C (ancient):

$$\frac{d(C_a \times \delta(C_a))}{dt} = F_{Cya} \times \delta(C_y) - carbw_a \times \delta(C_a) - ccdeg \times \delta(C_a)$$

(19)

Buried pyrite S (young):

$$\frac{d(PYR_y \times \delta(PYR_y))}{dt} = mpsb \times (\delta(S) - \Delta S) - pyrw_y \times \delta(PYR_y) - F_{PYRya} \times \delta(PYR_y)$$

(20)

Buried pyrite S (ancient):

$$\frac{d(PYR_a \times \delta(PYR_a))}{dt} = F_{PYRya} \times \delta(PYR_y) - pyrw_a \times \delta(PYR_a) - pyrdeg \times \delta(PYR_a)$$

(21)

Buried gypsum S (young):

$$\frac{d(GYP_y \times \delta(GYP_y))}{dt} = mgsb \times \delta(S) - gypw_y \times \delta(GYP_y) - F_{GYPya} \times \delta(GYP_y)$$

(22)

Buried gypsum S (ancient):

$$\frac{d(GYP_a \times \delta(GYP_a))}{dt} = F_{GYPya} \times \delta(GYP_y) - gypw_a \times \delta(GYP_a) - gypdeg \times \delta(GYP_a)$$

(23)

List of fluxes

Temperature dependence of basalt weathering:

$$f_{Tbas} = e^{0.061(T-T_0)}\{1 + 0.038(T - T_0)\}^{0.65}$$

(24)

Temperature dependence of granite weathering:

$$f_{Tgran} = e^{0.072(T-T_0)}\{1 + 0.038(T - T_0)\}^{0.65}$$

(25)

Temperature dependence of carbonate weathering:

$$g_T = 1 + 0.087(T - T_0)$$

(26)

Pre-plant silicate weathering: $f_{preplant} = f_T \cdot \sqrt{RCO_2}$

(27)

Plant-assisted silicate weathering: $f_{plant} = f_T \cdot \left(\frac{2RCO_2}{1+RCO_2}\right)^{0.4}$

(28)

Pre-plant carbonate weathering: $g_{preplant} = g_T \cdot \sqrt{RCO_2}$

(29)

Plant-assisted carbonate weathering: $g_{plant} = g_T \cdot \left(\frac{2RCO_2}{1+RCO_2}\right)^{0.4}$

(30)

Climate forcing for silicates:

$$f_{CO2} = f_{preplant}(1 - \min(VEG \cdot W)) + f_{plant} \cdot \min(VEG \cdot W)$$

(31)

$f_{CO2gran}$ and f_{CO2bas} result from the f_{CO2} function with plant-weathering feedbacks using f_{Tgran} and f_{Tbas} respectively.

Climate forcing for carbonates:

$$g_{CO2} = g_{preplant}(1 - \min(VEG \cdot W)) + g_{plant} \cdot \min(VEG \cdot W)$$

(32)

Vegetation feedback: $VEG = 2 \cdot E \cdot \frac{(CO_2ppm-10)}{(183.6+CO_2ppm-10)} \cdot \left(1 - \left(\frac{(T-T_0)}{T}\right)^2\right) \cdot \left(1.5 - 0.5(RO_2)\right) \cdot \frac{k_{fire}}{(k_{fire}-1+\max(586.2O_2(atm)-122.102\,,0))}$

(33)

Evolution of plants: $pevol = \left(k_{preplant} + \left(1 - k_{preplant}\right) \cdot W \cdot VEG\right)$

(34)

Basalt weathering: $basw = \%bas_0 \cdot k_{silw} \cdot f_{CO2bas} \cdot PG \cdot pevol \cdot BA$

(35)

Granite weathering:

$$granw = (1 - \%bas_0) \cdot k_{silw} \cdot f_{CO2gran} \cdot PG \cdot U \cdot pevol \cdot GA$$

(36)

Silicate weathering: $silw = basw + granw$

(37)

Carbonate weathering (young): $carbw_y = k_{carbwy} \cdot g_{CO2} \cdot PG \cdot U \cdot pevol \cdot LAC_{rel}$

(38)

Carbonate weathering (ancient): $carbw_a = k_{carbwa} \cdot g_{CO2} \cdot PG \cdot U \cdot pevol \cdot LAC_{rel}$

(39)

Oxidative weathering (young): $oxidw_y = k_{oxidwy} \cdot U \cdot \sqrt{RO_2}$

(40)

Oxidative weathering (ancient): $oxidw_y = k_{oxidwa} \cdot U \cdot \sqrt{RO_2}$

(41)

Transfer from C_y to C_a: $F_{Gya} = carbw_a - ccdeg$

(42)

Transfer from G_y to G_a: $F_{Gya} = oxidw_a - ocdeg$

(43)

Marine carbonate carbon burial: $mccb = silw + carbw$

(44)

Seafloor weathering is revised to include direct temperature dependence as with terrestrial basalt weathering. This assumes a direct relationship between surface temperature change and seafloor temperatures.

Seafloor weathering: $sfw = k_{sfw} \cdot D \cdot e^{0.061(T-T_0)}$

(45)

In COPSE, sulphur degassing is assumed to have the same controls as sulphur weathering, therefore the degassing terms are accounted for by larger weathering terms:

Pyrite sulphur weathering (young): $pyrw_y = k_{pyrwy} \cdot U \cdot \frac{PYR_y}{PYR_{y0}} \sqrt{RO_2}$

(46)

Pyrite sulphur weathering (ancient): $pyrw_a = k_{pyrwa} \cdot U \cdot \frac{PYR_a}{PYR_{a0}} \sqrt{RO_2}$

(47)

Gypsum sulphur weathering (young): $gypw = k_{gypw} \cdot U \cdot \frac{GYP_y}{GYP_{y0}} \cdot \frac{carbw}{carbw_0}$

(48)

Gypsum sulphur weathering (ancient): $gypw = k_{gypw} \cdot U \cdot \frac{GYP_a}{GYP_{a0}} \cdot \frac{carbw}{carbw_0}$

(49)

Transfer from GYP_y to GYP_a: $F_{GYPya} = gypw_a - gypdeg$

(50)

Transfer from PYR_y to PYR_a: $F_{PYRya} = pyrw_a - pyrdeg$

(51)

Gypsum sulphur burial: $mgsb = k_{mgsb} \cdot \frac{S}{S_0} \cdot \frac{CAL}{CAL_0}$

(52)

Organic carbon degassing: $ocdeg = k_{ocdeg} \left(\frac{G}{G_0}\right) \cdot D$

(53)

Carbonate carbon degassing: $ccdeg = k_{ccdeg} \left(\frac{C}{C_0}\right) \cdot D \cdot B$

(54)

Marine carbonate carbon burial: $mccb = silw + carbw$

(55)

Total organic carbon burial:

$$ocb = \frac{1}{\Delta B}\Big(carbw_y\left(\delta(A) - \delta(C_y)\right) + carbw_a\big(\delta(A) - \delta(C_a)\big) + oxidw_y\left(\delta(A) - \delta(G_y)\right) + oxidw_a\big(\delta(A) - \delta(G_a)\big) + ccdeg\big(\delta(A) - \delta(C_a)\big) + ocdeg\big(\delta(A) - \delta(G_a)\big)\Big)$$

(56)

Total pyrite sulphur burial:

$$pyrb = \frac{1}{\Delta S}\Big(gypw_y\left(\delta(S) - \delta(GYP_y)\right) + gypw_a\big(\delta(S) - \delta(GYP_a)\big) + pyrw_y\left(\delta(S) - \delta(PYR_y)\right) + pyrw_a\big(\delta(S) - \delta(PYR_a)\big) + gypdeg\big(\delta(S) - \delta(GYP_a)\big) + pyrdeg\big(\delta(S) - \delta(PYR_a)\big)\Big)$$

(57)

Other calculations:

Relative atmospheric O_2: $RO_2 = \frac{\frac{O}{O_0}}{\frac{O}{O_0} + k_{O2}}$

(58)

where $k_{O2} = 3.762$

Solar forcing: $S = \frac{S_0}{1 + 0.38\left(\frac{t}{\tau}\right)}$

(59) where $S_0 = 1368 Wm^{-2}$, $\tau = 4.55 \times 10^9$ years.

Present day values:		**Source:**
Marine organic carbon burial:	$k_{mocb} = 4.5 \times 10^{12}$ mol C yr^{-1}	COPSE
Pyrite sulphur burial:	$k_{mpsb} = 5.3 \times 10^{11}$ mol S yr^{-1}	COPSE
Gypsum sulphur burial:	$k_{mgsb} = 1 \times 10^{12}$ mol S yr^{-1}	COPSE
Silicate weathering:	$k_{silw} = 4.9 \times 10^{12}$ mol C yr^{-1}	for steady state

Seafloor weathering: $k_{sfw} = 1.75x10^{12}$ mol C yr^{-1} Mills et al. (2014)

Oxidative weathering (young): $k_{oxidwy}=7x10^{12}$ mol C yr^{-1} COPSE

Oxidative weathering (ancient): $k_{oxidwa}=7.75x10^{11}$ mol C yr^{-1} COPSE

Carbonate weathering (young): $k_{carbwy}=1.8x10^{13}$ mol C yr^{-1} COPSE

Carbonate weathering (ancient): $k_{carbwy}=2x10^{12}$ mol C yr^{-1} COPSE

Pyrite sulphur weathering (young): $k_{pyrw}=2.36x10^{11}$ mol S yr^{-1} COPSE

Pyrite sulphur weathering (ancient): $k_{pyrw}=2.9x10^{11}$ mol S yr^{-1} COPSE

Gypsum sulphur weathering (young) $k_{gypwy}=7.5x10^{11}$ mol S yr^{-1} COPSE

Gypsum sulphur weathering (ancient) $k_{gypwy}=2.5x10^{11}$ mol S yr^{-1} COPSE

Organic carbon degassing: $k_{ocdeg}=1.25x10^{12}$mol C yr^{-1} COPSE

Carbonate carbon degassing: $k_{ccdeg}=6.65x10^{12}$mol C yr^{-1} COPSE

Atmosphere and ocean CO_2: $A_0=3.193x10^{18}$ mol COPSE

Ocean sulphate:	$P_0=4x10^{19}$ mol
COPSE	
Atmosphere and ocean oxygen:	$O_0=3.7x10^{19}$ mol
COPSE	
Buried organic carbon:	$G_0=1.25x10^{21}$ mol
COPSE	
Buried carbonate carbon:	$C_0=6.6x10^{21}$ mol
COPSE	
Buried pyrite sulphur:	$PYR_0=1.8x10^{20}$mol
COPSE	
Buried gypsum sulphur:	$GYP_0=2x10^{20}$ mol
COPSE	
Forcings:	**Attributes:**
Solar forcing:	$S = \frac{S_0}{1+0.38\left(\frac{t}{\tau}\right)}$
	where S_0 = 1368Wm^{-2}, τ=4.55x10^9 years.
Relative global CO_2 degassing:	$D = 1$ for present day
Relative uplift rate:	$U = 1$ for present day
Evolution of land plants:	$E = 1$ for present day
Weathering effect of plant evolution:	$W = 1$ for present day
Carbonate burial depth:	$B = 1$ for present day
Relative basaltic area:	$BA = 1$ for present day
Relative total land area:	LA_{rel} = 1 for present day
Relative carbonate land area:	LAC_{rel} = 1 for present day

Relative granite area: $GA = LA - LAC - BA_{cont}$

where BA_{cont} is the total basaltic area on continents (i.e. total basaltic area minus island arc and ocean island contributions) and LA and LAC are the total land area and carbonate land area respectively, calculated by scaling the relative areas to the present day areas.

Paleogeographical runoff effect: $PG = 1$ for present day

Starting conditions

The model reservoir of ancient carbonates, C_a, is by far the largest store of carbon, therefore its assumed isotopic composition at the start of the model run will influence the relative carbon burial rates for this time. This parameter is set so that organic C burial rates and oxygen concentration return to present day values at the end of the run (0Ma). This requires $\delta(C_{astart}) = 1.16$ for the GEOCARB δ^{13}Cinput, and $\delta(C_{astart}) = -0.56$ for the GTS2012 input.

Model output

Figure A2 shows IMB-COPSE model output for 3 combinations of input parameters:

1) δ^{13}C and δ^{34}S inputs follow GEOCARBSULF. Shown in green.
2) δ^{13}C input follows GEOCARBSULF, δ^{34}S inputs follow Algeo et al., (2015). Shown in orange.
3) δ^{13}C input follows GTS2012 (Saltzman and Thomas, 2012), δ^{34}S inputs follow Algeo et al., (2015). Shown in red.

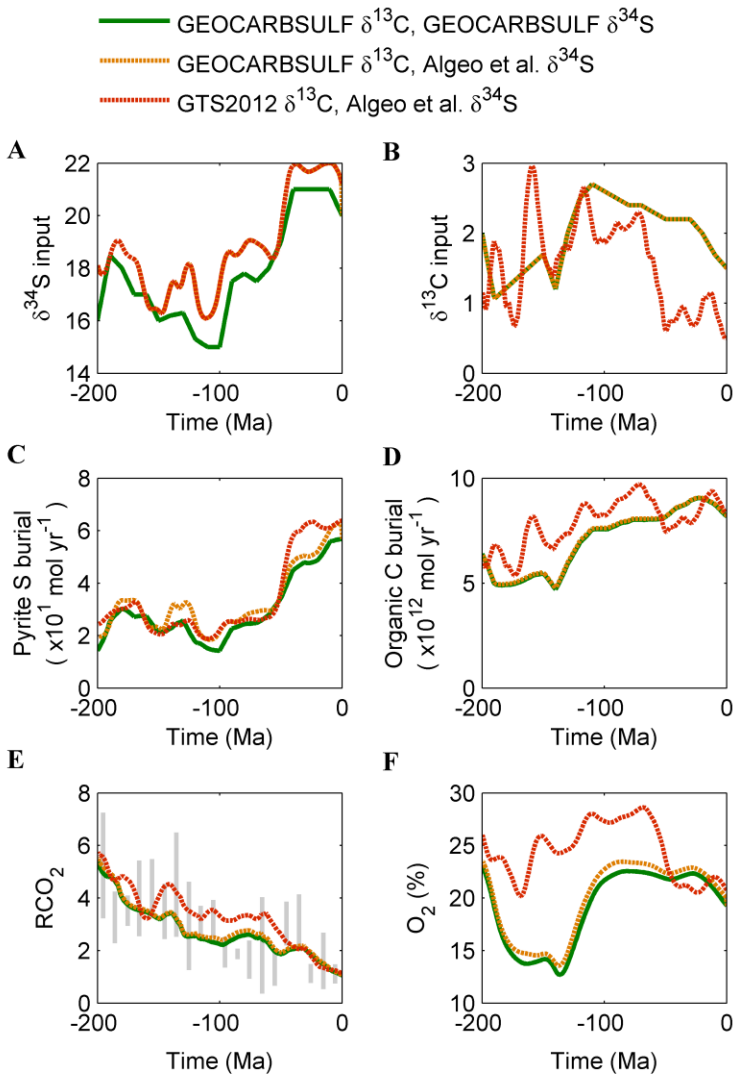

Figure A2. IMB-COPSE model output for different isotope input scenarios. Relative atmospheric CO_2 concentration plotted against compilation of Park and Royer (2011).

Under the GEOCARBSULF inputs, the IMB-COPSE model predicts very similar variations in atmospheric oxygen to the original GEOCARBSULF model (Berner, 2009; see manuscript). When $\delta^{34}S$ input is altered to follow Algeo et al., (2015), oxygen variation is only slightly affected, owing to the minor alteration to the input (around one

5th of the range), and to the significantly smaller fluxes of oxygen associated with the sulphur system when compared to carbon. When the $\delta^{13}C$ input parameter is also altered, predicted oxygen concentration is significantly changed, and is higher over the model timeframe. This stems from the assumption that Mesozoic $\delta^{13}C$ was higher than present, equating to greater organic carbon burial in this model variant.

APPENDIX 3: ADDITIONAL MODEL EXPERIMENTS

Sensitivity of O_2 predictions to input parameters other than carbonate $\delta^{13}C$

In the manuscript we show extreme sensitivity of modelled oxygen predictions to carbonate $\delta^{13}C$ inputs. In figure A3 we test additional uncertainty by including error estimates for other model processes. The grey area shows the extent of the range of model predictions when run with $\pm 1\sigma$ variation in carbonate $\delta^{13}C$, but also with variation between the minimum and maximum estimates for the rate of volcanic CO_2 degassing and the global area of weatherable volcanic rocks. This mirrors the sensitivity window shown in Mills et al., (2014). The effects on atmospheric oxygen predictions are minimal when compared to the variation assumed in carbonate $\delta^{13}C$ alone (blue dashed lines). It has been shown (Royer et al., 2014) that multi-parameter error analysis on all input parameters (~70 for GEOCARBSULF) can result in similar uncertainty ranges for model O_2 predictions as calculated here by varying only the $\delta^{13}C$ input. The grey error window we show could be extended using this method (although many of these assumed error windows are themselves arbitrary – the degassing rate and carbonate $\delta^{13}C$ curve used in this modelling are significantly outside the error range used by Royer et al., (2014)), but the median predictions are not altered by such analyses.

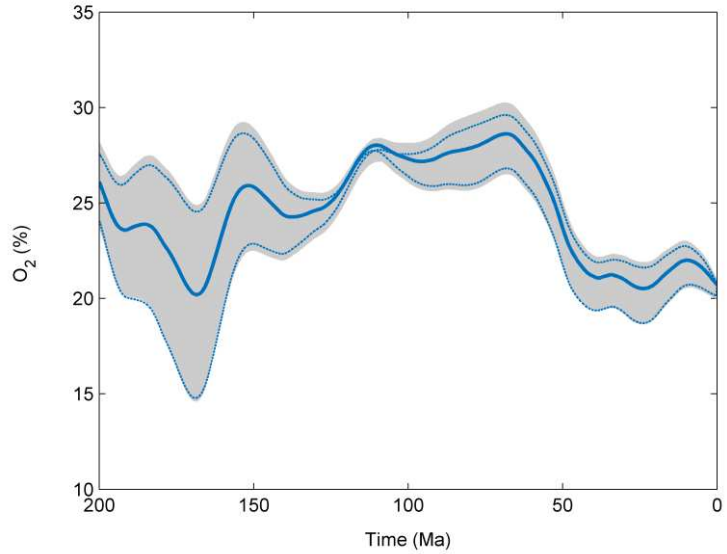

Figure A3. Model error window (grey) when subject to max/min variation in inputs for carbonate $\delta^{13}C$, volcanic CO_2 degassing rate and weatherable area of volcanic rocks. See Mills et al., (2014) for details of these processes. Compared to model error window under $\pm 1\sigma$ in carbonate $\delta^{13}C$ input (blue dashed lines).

Model sensitivity to carbonate reservoir variations.

Our model assumes an increase in the degassing rate of carbonates at ~140Ma, aiming to represent the subduction of deep ocean carbonate deposits after the evolution of calcareous plankton (burial depth forcing B above, following from GEOCARB modelling). However, carbonate subduction may be more dependent on longer term basin dynamics and may therefore produce a destabilizing effect on the carbon cycle (Edmond and Huh, 2003). In figure A4 we replace the B forcing with a new flux from the young carbonate reservoir to the atmosphere/ocean. This represents tectonic control of carbonate subduction and follows Edmond and Huh (2003; panel A). As discussed by these authors, this flux can have a considerable impact on model CO_2 predictions. This follows from the

idea that the modern day steady state does not include some significant past processes. The impact on our oxygen predictions is however relatively small: the increase in carbon fluxes only represents around 10% of the total gross throughput, and therefore does not greatly alter the mass balance calculation or O_2 (see manuscript).

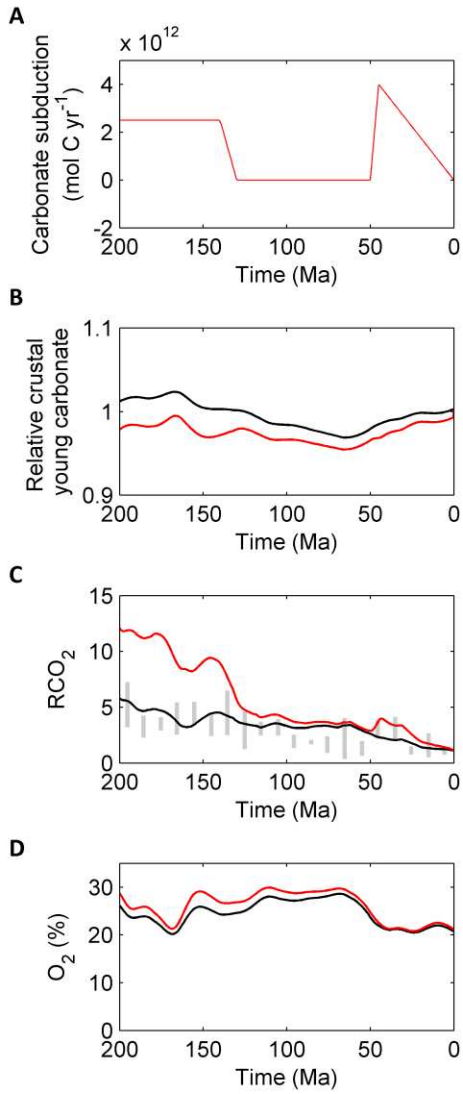

Figure A4. Model configured with additional carbonate subduction flux from young carbonates to atmosphere/ocean (red). Compared to original model (black).

Model sensitivity to pyrite burial constraints.

The quantity f_{pyr} represents pyrite burial as a fraction of total sulphur burial. In GEOCARB and COPSE modelling f_{pyr} is around 0.3-0.4 at the present day. It has however been suggested, based on direct estimation of the sulphate burial rate, that f_{pyr} may have been as high as 0.9 and stable at this fraction for the whole Phanerozoic (Halevy et al., 2012). To close the isotope mass balance under this constraint requires a fixed time-evolution of the isotopic composition of sulphate inputs (figure A5, panel A), although this is not supported by available data on the composition of sulphur in coals (Canfield, 2013). In figure A5 we run the model with an imposed $\delta^{34}S$ of sulphate inputs, and an increased rate of pyrite burial at present day (Halevy et al., 2012). Variation in oxygen predictions are again small. This is because the rate of oxygen production from pyrite burial is still much smaller than via organic carbon burial (around 20%), and also because the higher and more stable rate of pyrite burial in the altered model acts to reduce the overall variation in oxygen production rates.

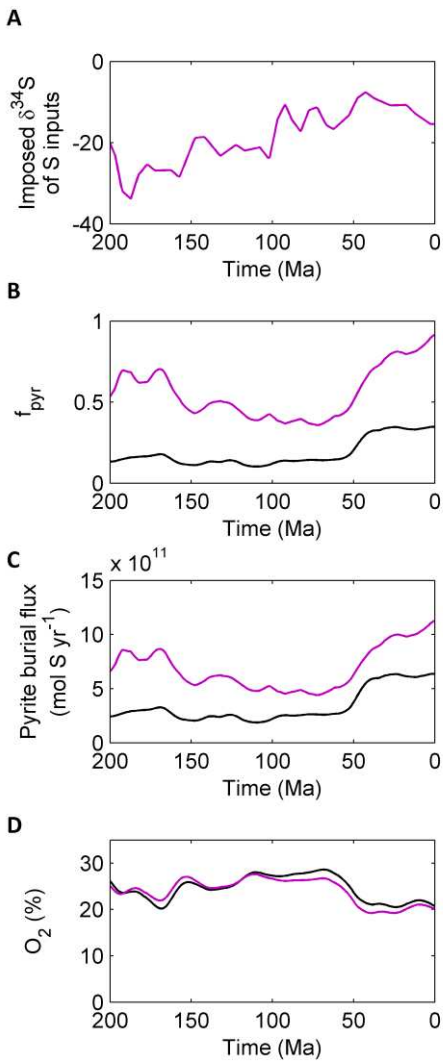

Figure A5. Model configured with hig*her rate of pyrite burial and imposed* δ^{34}S value for sulphate inputs (purple). Compared to original model (black).

ADDITIONAL REFERENCES

Berner, R. A., 1991, A model for atmospheric CO_2 over Phanerozoic time: American Journal of Science, v. 291, p. 339-376.

Berner, R. A., 1994, Geocarb II: A revised model of atmospheric CO_2 over Phanerozoic time: American Journal of Science, v. 294, p. 56-91.

Berner, R. A., and Kothavala, Z., 2001, Geocarb III: A revised model of atmospheric CO_2 over Phanerozoic time: American Journal of Science, v. 301, p. 182-204.

Canfield, D. E., 2013, Sulfur isotopes in coal constrain the evolution of the Phanerozoic sulfur cycle. PNAS v. 110, p. 8443-8446.

Edmond, J. M. and Huh, Y., 2003, Non-steady state carbonate recycling and implications for the evolution of atmospheric pCO_2. EPSL v. 216, p. 125-139.

Halevy I, Peters S. E. and Fischer W. W., 2012, Sulfate burial constraints on the Phanerozoic sulfur cycle. Science v. 337, p. 331–334.

Park, J., and Royer, D. L., 2011, Geologic constraints on the glacial amplification of Phanerozoic climate sensitivity: American Journal of Science, v. 311, p. 1-26.